Submicron imaging of buried integrated circuit structures using scanning confocal electron microscopy

Sean P. Frigo[a)]
Department of Physics and Astronomy, Northern Arizona University, P.O. Box 6010, Flagstaff, Arizona 86011-6010

Zachary H. Levine
National Institute of Standards and Technology, Gaithersburg, Maryland 20899-8410

Nestor J. Zaluzec
Materials Science Division, Argonne National Laboratory, 9700 S. Cass Ave., Argonne, Illinois 80439-4838

Two-dimensional images of model integrated circuit components were collected using the technique of scanning confocal electron microscopy. For structures embedded about 5 μm below the surface of a silicon oxide dielectric, a lateral resolution of 76 ± 9 nm was measured. Elemental mapping via x-ray emission spectrometry is demonstrated. A parallax analysis of images taken for various tilt angles to the electron beam allowed determination of the spacing between two wiring planes. The results show that scanning confocal electron microscopy is capable of probing buried structures at resolutions that will be necessary for the inspection of next-generation integrated circuit technology. © *2002 American Institute of Physics.* [DOI: 10.1063/1.1506010]

Transmission and scanning transmission electron microscopes (TEM and STEM, respectively) have been developed into a suite of powerful high resolution and element-specific imaging instruments.[1] However, strong beam interactions such as multiple Rutherford and plasmon scattering cause significant decreases in image resolution with increasing specimen thickness.[2,3] Thus, to achieve good imaging conditions in a TEM/STEM requires extensive sample processing, i.e., thinning, to be performed.

In a number of situations it would be desirable to image much thicker specimens—on the order of microns thick—albeit at lesser resolution than the optimum afforded by a TEM or STEM, which is around 0.2 nm. Engineered integrated circuits are a prime example of this type of specimen. They consist of layers containing interconnect wires in 4–8 planes and vertical vias providing connections between the planes. There is a strong interest in performing nondestructive imaging for the characterization and analysis of integrated circuit devices. Using scanning transmission x-ray microscopy (STXM), a metrology study has reported a measured lateral [two-dimensional (2D)] instrumental resolution of 200 nm,[4] and a tomography study reported lateral and volumetric (3D) resolutions of 60 and 140 nm, respectively.[5]

An electron microscopy imaging technology, scanning confocal electron microscopy (SCEM),[6] has been developed to image thick samples at resolutions better than that currently achievable using conventional electron microscopies. The SCEM[6] is an electron optical analog of the scanning confocal optical microscope (SCOM).[7] The instrument used in this work, schematically shown in Fig. 1, is a modification of the advanced analytical electron microscope at Argonne National Laboratory and is described in detail elsewhere.[6,8]

The illumination source employs an aperture-limited, cold field emission electron gun operating at 300 kV and produces a nominal 0.1 nA electron probe. The probe was focused by single condenser lens onto the specimen of interest. The scattered distribution from the specimen was subsequently transferred by a single postspecimen lens onto an aperture-limited detector consisting of a yttrium–aluminum–garnet scintillator crystal and matched photomultiplier tube.

The SCEM was operated in an asymmetric illumination/detection mode, where the illumination semiangle α for the measurements was about 15 mrad, while the collection semiangle β was greater than 150 mrad. Images were formed by rastering the incident electron probe in an x,y pattern over the specimen, while simultaneously measuring the descanned transmitted signal on the single postspecimen detector into a digital storage system. Scan amplitudes were stepwise ad-
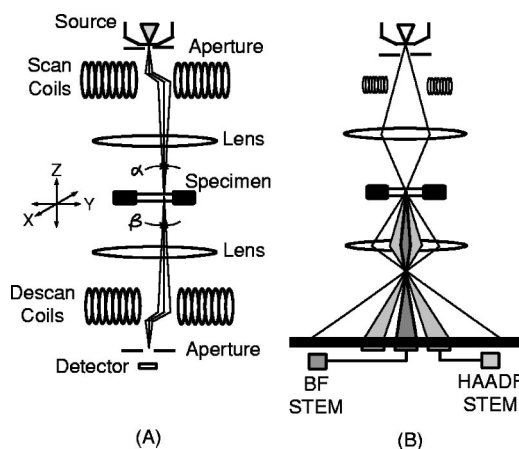

FIG. 1. Comparison of SCEM and STEM imaging geometries. The optical configuration of the SCEM is shown on the left (A), while typical STEM modes are shown on the right (B).
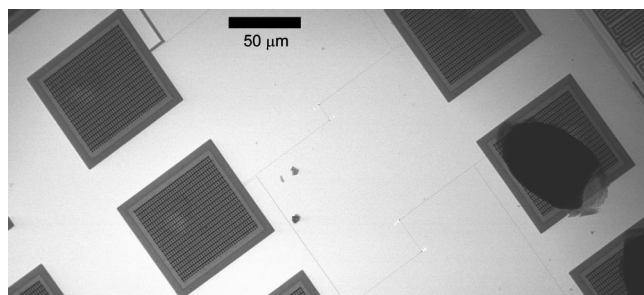
[a)]Electronic mail: sean.frigo@nau.edu

FIG. 2. Wide-field image. The square structures are bond pads containing fields of vias. Interconnects buried in an SiO$_2$ matrix connect the bond pads. The interconnects and vias are clearly visible in the electronic image. The field of view covers 450 μm by 225 μm, and the bond pad edges are 80 μm long.
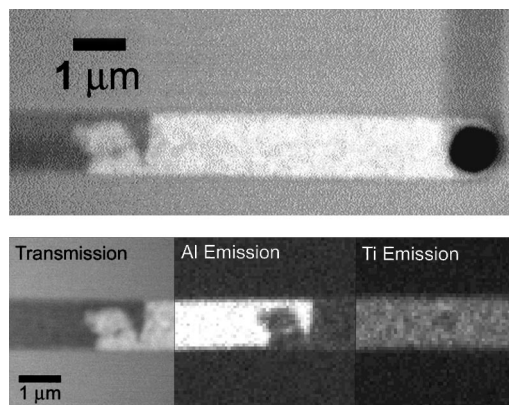

FIG. 3. An electromigration void created by current induced motion of the aluminum layer in the interconnect. The dark circle is an end-on view of a tungsten via connecting interconnects lying in two different planes. An analysis of a vertical intensity profile across the void yields an edge half-width of about 80 nm. The void detail observed using transmission and corresponding detected Al and Ti $K\alpha$ x-ray emission are shown in the left, middle and right images at the bottom, respectively. The Ti is contained in diffusion barrier layers, located above and below the Al layer, and which remain intact after Al electromigration.

justable to cover the range of about 1 mm to about 1 nm in x and y, respectively. Both pre- and postspecimen scan/descan coils were employed to insure the reciprocity of the source and detector, particularly at low magnifications.

The SCEM optical configuration is similar to that of the STEM.[1] Generally, in STEM the optics are preset so that one either measures the directly transmitted signal in bright field mode, or a limited annulus of scattered signal in high angle annular dark field mode as shown in Fig. 1. In contrast, in SCEM we collect nearly all of the scattered signal. This results in a better signal to noise ratio and images which exhibit less resolution degradation, due to minimal effects of chromatic aberration in SCEM relative to that in conventional TEM/STEM. Thus, STEM operations are subsets of the more general SCEM mode as their corresponding signals are subsets of the confocally collected data, as is seen from the geometry in Fig. 1. In this work we report solely on the use of SCEM in viewing buried defects rather than depth sectioning as is often, but not exclusively, employed in SCOM configurations.[7] This is because the depth of field of the SCEM implementation used in this study was limited by the angular acceptance of the postspecimen optics.

The specimen in this work was a section from an accelerated life cycle test wafer containing model structures having a 0.35 μm design rule at the transistor level. The section was thinned via polishing and then dimpled and ion milled from the substrate side to yield a 400 μm circular region of free-standing SiO$_2$ matrix containing interconnects and bond pads. A three-dimensional image created from STXM data of a specimen from the same test suite and with similar geometry is shown in Ref. 5.

A portion of a wide-field view of the sample is shown in Fig. 2 which represents one half of a 1920 by 1920 pixel image covering an area 450 μm by 450 μm and acquired at 333 ms/line. The square structures visible in the figure are aluminum bond pads. They contain arrays of tungsten vias that connect to corresponding Al squares lying in a plane about 1 μm below. The dark oval visible on one bond pad is solder left from the attachment of a contact lead. Interconnects between the bond pads are discernible as fine lines between the pads. The interconnects are buried in an SiO$_2$ matrix, which corresponds to the brighter parts of the image. It is easy to discern the lighter silicon oxide and aluminum from the heavier tungsten in the bond pad region. This follows from contrast-generating Rutherford scattering events

whose cross sections increase approximately as the atomic number squared.[1] We also note that the channels in the upper right hand corner of Fig. 2 lie outside the dimpled region where there are tens of microns of Si substrate, further illustrating the capability of SCEM to produce images where substrate thinning via polishing is the *only* preparation.

When the test structure was subjected to accelerated lifetime conditions, current sent through two bond pads induced electromigration in an interconnect. This created a void near a junction with a tungsten via, the detail of which is shown in Fig. 3. Here, we are able to resolve detailed fine structures present in the void end farthest away from the via. The image intensity along a line through the horizontal interconnect in Fig. 3 shows levels in the interconnect and void regions relative to those in the matrix to be 0.8 and 1.2, respectively. This profile indicates residual material and a slight decrease in the void thickness along the direction away from the via.

An analysis of the intensity across a vertical line crossing the void edge yields an edge width of 76$\pm$9 nm. (All uncertainties quoted herein are total with a 95% confidence interval.) This value is an upper bound for the resolution in the plane of the void because the contrast-producing region has a nonzero thickness and there may be lateral density variations. Both will make any edges in our sample appear less sharply defined. From the parallax analysis presented below, we find the beam passes through about 5 μm of SiO$_2$ before the void. We expect achievable lateral resolutions around 80–100 nm for this distance.[6]

Transmission contrast reflects the spatial variation in atomic number. Contrast is also observable via traditional elemental mapping from detection of electron-induced x-ray emission via energy dispersive spectroscopy. We show this capability in Fig. 3 with images taken of the void region using the transmitted electron signal as well as Al and Ti $K\alpha$ emission. The data were collected over 0.3 sr using an Oxford Instruments windowless Si(Li) x-ray detector whose axis was elevated 20° to the specimen surface. At 1 s/pixel,
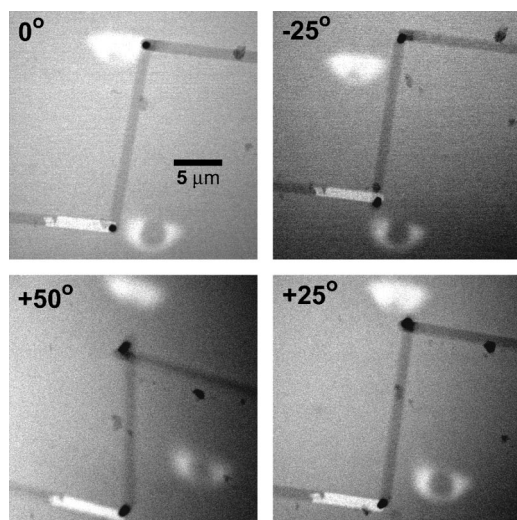
FIG. 4. Representative images from the tilt series for angles of $0°$, $-25°$, $+25°$, and $+50°$. The light circular regions are markers consisting of craters with Ti islands produced by a focused ion beam. They lie in a third plane above the two interconnect planes. The change in marker positions and increasing via lengths with increasing tilt angle are clearly discernible.
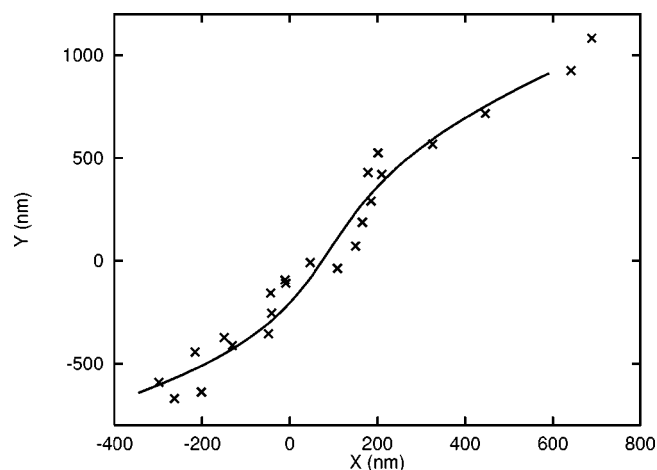

FIG. 5. Parallax analysis results. The observed intersection positions (x,y) of interconnect centerlines in the 2D projection plane are plotted with crosses. The line is the intersection projection function fit to the observed data. The fit yields a value of $h = 0.86 \pm 0.20$ μm for the interlayer spacing.

each 64 by 64 pixel x-ray emission image required just over 1 h to collect. Elemental mapping may help to answer questions such as the role of precipitates in void formation.[9] We see in our case that the Ti liner layers remain intact and the Al in between has moved. This is also observable in the tomographic reconstruction of a void in a similar sample.[5]

We also acquired images of interconnect segments as a function of orientation by tilting the specimen over the range of $-50°$ to $+50°$ in $5°$ increments. Sample images for angles of $0°$, $\pm 25°$, and $50°$ are shown in Fig. 4. A parallax analysis of the tilt series was performed according to the techniques outlined in Ref. 10. The alignment portion of the analysis yielded orientation angle values of ϕ, η, and θ_0 to be $63.234°$, $-4.677°$, and $-2.392°$, respectively. Next, it is necessary to identify a reference point on each 2D image which projects back onto the same 3D point in the sample. A particular via center is suitable. Then, (x,y) coordinates of the intersection of the centerlines of a particular pair of wires are determined for nearly every 2D view. The six-parameter fit is used to generate a function containing a 1-parameter prediction of the (x,y) position of the wire intersection in each 2D image. This latter parameter is the center-to-center interlayer spacing h. Fitting to the observed intersection coordinate data, h is found to be 16.1 ± 2.0 pixels, or 0.86 ± 0.20 μm using the linewidth obtained from x-ray imaging.[5] The fit function is plotted with the data in Fig. 5. For this interlayer spacing, we estimate the distance from the void to the surface containing the focused ion beam markers to be 5.0 ± 1.0 μm from inspection of the $+50°$ tilt image.

We have demonstrated the ability to image buried interconnect structures that are part of an integrated circuit using a scanning confocal electron microscope. We were able to measure an object within a matrix located 5 μm below an overlayer at a lateral resolution below 80 nm. We were also able to perform elemental mapping via x-ray emission. A parallax analysis of a tilt series shows that one can also determine interlayer spacings. These results show that using SCEM can reduce the need for sample thinning and open the door toward imaging micron-sized 3D structures such as integrated circuit devices at sub-100 nm lateral resolutions.

[1] L. Reimer, *The Physical Principles of the Transmission Electron Microscope*, 2nd ed. (Springer, Berlin, 1997).
[2] T. Groves, Ultramicroscopy **1**, 15 (1975).
[3] L. Reimer, Ultramicroscopy **31**, 169 (1989).
[4] X. Su, C. Stagarescu, G. Xu, D. E. Eastman, I. McNulty, S. P. Frigo, Y. Wang, C. C. Retsch, I. C. Noyan, and C.-K. Hu, Appl. Phys. Lett. **77**, 3465 (2000).
[5] Z. H. Levine, A. R. Kalukin, M. Kuhn, S. P. Frigo, I. McNulty, C. C. Retsch, Y. Wang, U. Arp, T. Lucatorto, B. D. Ravel, and C. Tarrio, J. Appl. Phys. **87**, 4483 (2000).
[6] N. J. Zaluzec, "A Scanning Confocal Electron Microscope," US patent submitted.
[7] "Foundations of Confocal Scanned Imaging in Light Microscopy," in *The Handbook of Biological Confocal Microscopy*, edited by J. Pawley (IMR, University of Wisconsin-Madison, Madison, Wisconsin, 1988), pp. 1–13.
[8] N. J. Zaluzec, *MicroBeam Analysis-1991*, edited by D. G. Howitt (San Francisco Press, San Francisco, 1991), p. 137.
[9] C.-K. Hu, K. P. Rodbell, T. D. Sullivan, K. Y. Lee, and D. P. Bouldin, IBM J. Res. Dev. **39**, 465 (1995).
[10] Z. H. Levine, S. Grantham, S. Neogi, S. P. Frigo, I. McNulty, C. C. Retsch, Y. Wang, and T. B. Lucatorto, J. Appl. Phys. **90**, 556 (2001).